12th IEA Heat Pump Conference 2017

Heat Pump driven by a Small-Scale Oil-Free Turbocompressor – System Design and Simulation

Cordin Arpagaus[a]*, Frédéric Bless[a], Stefan S. Bertsch[a], Adeel Javed[b], Jürg Schiffmann[b]

[a]*NTB University of Applied Sciences of Technology Buchs, Institute for Energy Systems, Werdenbergstrasse 4, 9471 Buchs, Switzerland*

[b]*EPFL, Laboratory for Applied Mechanical Design, Rue de la Maladière 71b, 2002 Neuchâtel, Switzerland*

Abstract

Small-scale oil-free turbocompressors driven by high-speed electric motors and supported on refrigerant vapor bearings represent a promising technology to increase the performance of domestic heat pumps. Gas bearings enable high rotational speeds with low mechanical losses. Furthermore, turbocompressors can reach high compression efficiencies and offer a compact and lightweight design.
This paper evaluates the performance of a heat pump using a small-scale radial turbocompressor rotating on gas bearings. The turbocompressor has been optimized for R134a and achieves pressure ratios ion the order of 1.5 to 3.5 at rotational speeds of 160 to 280 krpm with isentropic efficiencies of up to 75%. The impeller diameter is 15.2 mm. A system model of the heat pump has been programmed in the Engineering Equation Solver (EES) software. The model uses effectiveness-NTU models for the heat exchangers and polynomial fit approximations for the non-dimensional compressor map data. The heat pump produces 4.0 kW of 30°C water from 10°C ground heat with a predicted COP of 8.1 and 53.4% 2nd law efficiency.
Simulation results, the design of the turbocompressor impeller, as well as the layout of the experimental setup are presented. First experimental measurement results will be expected in the beginning of 2017. The system serves as a proof of concept before stepping forward to a two-stage heat pump cycle with two turbocompressors reaching heat sink temperatures of 55 to 65°C.

Keywords: residential heat pump; small-scale oil-free turbocompressors; gas bearings; system design; simulation, R134a

1. Introduction

1.1. Motivation

According to the IEA [1], the worldwide fraction of energy consumed by the residential sector accounts for 29%, out of which 53% are used for space heating and 16% for water heating. Heat pumps have been identified as a key-technology to reduce the energy consumption in households. In spite of the wide use of heat pumps in the residential sector, there is still considerable potential for performance improvement and corresponding research needs. For example, today's brine/water heat pumps reach COP values of 4.5 [2] at B0/W35 test conditions (EN14511 [3]), which corresponds to a 2nd law efficiency of 51%. By 2050, the Swiss Federal Office for Energy Research [4] targets a 2nd law efficiency of 65% or COP of 5.7 at the same conditions.

* Corresponding author. Tel.: +41-81-755-34-94; fax: +41-81-756-54-34.
E-mail address: cordin.arpagaus@ntb.ch.

It is known that the major exergy losses in single stage heat pumps occur in the compressor (about 50%) [5, 6]. Compressors with the highest possible efficiency are therefore desirable to improve heat pump performance. Today's residential heat pumps are mostly equipped with scroll, rotary or reciprocating compressors that reach isentropic efficiencies in the order of 60% to 70% [7]–[9]. However, such compressors require oil for lubrication. The presence of oil may lead to oil degradation at high gas temperatures and to efficiency reduction in compression and heat transfer. In addition, oil migration within multi-stage cycles demands sophisticated oil management systems [5].

Turbocompressors, on the other hand, can be realized without oil, which is established technology in large scale heat pumps with heating capacities above 150 kW [10], [11]. Oil-free operation bears also the advantage in the design of advanced multi-stage heat pump cycles for better usage of the exergy and COP improvement compared to single stage cycles [12]–[16].

Small-scale, compact and lightweight turbocompressors designed for domestic heat pump applications (e.g. < 6 kW output power) are gradually becoming ready for the market [17], [18], especially thanks to the availability of high-speed electric motors. As stated by Schiffmann and Favrat [12], [19], appropriate small-scale oil-free turbocompressors for domestic heat pumps require the ability to operate on a wide range of inlet pressure, pressure ratios, and refrigerant mass flows. There is still optimization potential in the bearing and sealing design to reach acceptable long lifetime, high rotational speeds, and short maintenance times [20]. Further challenges are the limited pressure ratios [21] and the ability to manufacture small tip clearances [22]. Several authors have studied the feasibility to integrate small-scale turbocompressor technology in domestic heat pumps [6], [12], [13], [23], [24], [20]–[22], [25]–[28]. Table 1 gives a summary of those research studies.

Small-scale oil-free radial turbocompressors rotating on gas bearings have been identified as a promising way to significantly increase the performance in domestic heat pumps [13], [23], [25], [26]. The dynamic gas bearing technology runs on vapor phase refrigerant which builds gas cushions through its own rotation and enables ultra-high rotational speeds with almost wear-free operation, long lifetime, as well as minimal noise and vibration emission [6], [18], [29].

Schiffmann and Favrat [6], [12], [13], [23] experimentally demonstrated the technical feasibility of a small-scale oil-free single stage direct driven turbocompressor (up to 210 krpm and pressure ratio 3.3) supported on herringbone grooved journal bearings lubricated with vapor phase refrigerant fluid R134a. Internal isentropic compressor efficiencies of up to 79% were reached on a vapor phase test rig with several compressor prototypes and impeller diameters of about 20 mm. Based on a similar compressor design methodology, Carré et al. [24] from the same research group integrated a twin-stage oil-free radial compressor (rotating on the same shaft) in a two-stage air/water heat pump and demonstrated its technical feasibility for space heating application. A COP of 2.7 was experimentally reached at test conditions A-7/W35.

Recently, Javed et al. [22], [26] presented a detailed methodology on the design of miniature turbocompressors for wide-range operation in the presence of a large tip-clearance of 80 µm and associated tip-leakage flow. The compressors are able to theoretically achieve isentropic efficiencies of up to 77% at design point conditions (R134a, 0.02 kg/s, pressure ratio 2.3). Those predicted turbocompressor map data were used by Arpagaus et al. [25] to simulate the performance of a 6.5 kW two-stage heat pump using two heat sources at different temperature levels (1st heat source at 5°C and 2nd heat source at 30°C). The addition of 30% 2nd heat source resulted in a 19% higher COP compared to a system without 2nd source heat.

Table 1. Research studies on small-scale turbocompressors for domestic heat pumps (n.a. = not available, A: air, B: brine, W: water, E: experimental, S: simulation)

Heat pump system	Pressure ratio [-] *Isentropic compressor efficiency [%]*	Speed [krpm] *Impeller diameter [mm]*	Bearing type *Refrigerant*	Operating conditions *Heating capacity [kW]*	COP [-]	Ref.
Vapor phase test rig	1.5 to 3.3 *Up to 79*	150 to 210 *20*	Gas bearing *R134a*	(A-12/W60) to (A12/W40) *7 to 16*	2.5 to 5.0 (E)	[6], [12], [13], [23]
Two-stage with twin-stage compressor	2.3 and 2.7 *82 to 88*	180 *2 x 20*	Gas bearing *R134a*	(A-7/W35) *10*	2.7 (E)	[24]
Two-stage with two heat sources and two compressors	1.5-3.5 *Up to 77*	160 to 270 *2 x 15*	Gas bearing *R134a*	(B5/W30/W55) *6.5*	4.3 (S)	[22], [25], [26]

One-stage	2.5 *n.a.*	142 to 200 *21*	Ball bearing *Butane (R600)*	(B9/W28) *4 to 20*	9.7 (E)	[21], [27]
Three-stage compressor system	2 x 1.8 and 1.7 (overall 4.7) *59, 62 and 70* *(overall 68)*	180 to 195 2 x *23 and 21*	Ball bearing *Isopentane (R601)*	(W45/W100) *7.5*	2.3 (E)	[20], [28]

Wyssen et al. [21] built a 4 to 20 kW heat pump system with a turbo compressor rotating on ball bearings optimized for small temperature lifts of 10 to 24°C using butane (R600). A heating COP of 9 and 15 was reported for temperature lifts of 20°C and 10°C, respectively. Within the studied temperature lift range the 2nd law efficiency remained close to 60% (at 10°C evaporation temperature). In a subsequent work, Gasser et al. [27] reported a heating COP of 9.7 with a 2nd law efficiency of 62.7% for a floor heating application (B9°C/W28°C). The heat pump performance at temperature lifts below 25°C was significantly higher compared to a similar heat pump driven by a piston compressor.

Van Gerner et al. [20], [28] developed a heat pump demonstrator for aerospace application with a lightweight (~ 2 kg) three-stage centrifugal compressor system running on isopentane (R601a) and ball bearings. The three turbocompressors are divided in serial configuration and deliver a total pressure ratio of about 4.7. At the target operating conditions (W45°C/W100°C, heat input 5 kW) a COP of 2.3 was experimentally measured. The study showed that a heat pump concept with three small-scale turbocompressors in a serial configuration is feasible.

However, the lifetime of ball bearings is not yet sufficient for space applications. Gas bearings, on the other side, provide longer lifetime due to the contactless design [20], [28], in particular at high rotational speeds [13].

The review of research for the last 10 years reveals that the studies differentiate in terms of the applied number of compressors (one, two, three), their system arrangement (single-, twin-, three-stage), the applied refrigerant (R134a, R600, R601) and bearing types (gas, ball), the rotational speeds (140 to 270 krpm), the impeller size (15 to 21 mm), the pressure ratios (1.5 to 3.5) and temperature lifts (20 to 72°C).

The aim of this paper is to theoretically evaluate the performance and operating range of a one-stage heat pump driven by a small-scale single-stage turbo compressor with 15 mm impeller diameter rotating on gas bearings optimized for R134a [26]. The system serves as a proof of concept before stepping forward to a two-stage heat pump with two heat sources and two turbocompressors reaching sink temperatures of 55 to 65°C [25].

1.2. System description

Figure 1 shows the schematic diagram of the heat pump cycle along with the corresponding p-h diagram. The design point conditions represent a potential domestic space heating application in low-energy houses. Warm water of 30 ± 5°C is produced using a ground heat source of 10 ± 5°C. The heat capacity is 4.0 ± 0.5 kW. The cycle uses a brine-heated evaporator and a water-cooled condenser. The suction line heat exchanger (SHX) ensures superheating of the vapor entering the compressor and subcooling of the liquid exiting the condenser. The refrigerant passes through a suction line accumulator (SLA) before entering the compressor as a protection to prevent injection of liquid droplets into the high-speed radial compressor [29]. The discharge gas from the compressor is directed into the condenser. The refrigerant flows back via the expansion valve to the evaporator.

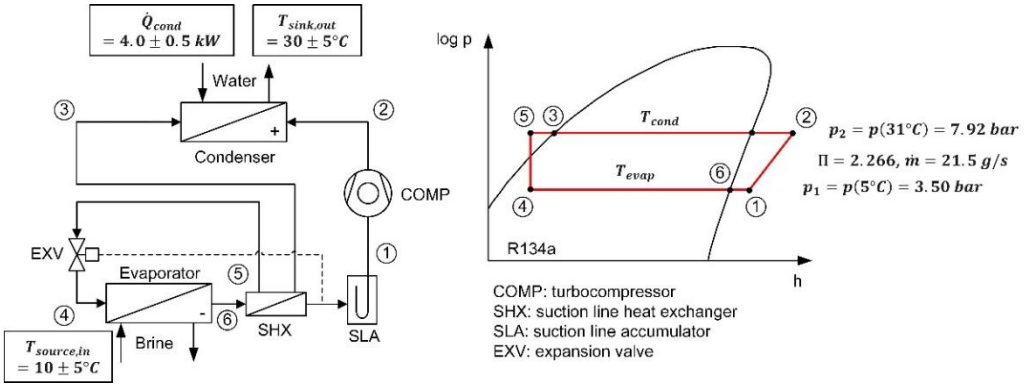

Fig. 1. Schematic and p-h diagram of the one-stage heat pump cycle at design conditions (B10°C/W30°C, 4.0 kW).

1.3. Design point conditions

The oil-free turbocompressor has been designed specifically to meet the design requirements of the 1st stage of a two-stage heat pump [25] (see design conditions in Table 1). Details about the compressor design procedure are described in Javed et al. [22], [26]. For the space heating application of the present one-stage heat pump higher temperature conditions were selected as heat pump design point conditions, as illustrated in Figure 1.

Table 1. Design conditions of the turbocompressor, data from Javed et al. [22], [26].

Parameter	Symbol	Value	Unit
Mass flow rate R134a	$\dot{m}$	0.02	kg/s
Pressure ratio	Π	2.30	-
Inlet pressure	p	2.72	bar
Isentropic Efficiency	η	76.5	%
Design speed	n	227,000	rpm
Electrical power	W_{el}	0.49	kW
Tip diameter of the impeller	D	15.24	mm

The turbocompressor is optimized for R134a, as it allows acceptable compressor diameters, large tip clearance of 80 µm and moderate pressure ratios [22]. Propane or isobutene could also be considered for this application, as they are promising natural refrigerants and achieve higher temperature lifts. Compared to R290, the rotational speed with R134a is considerably lower, allowing higher electric efficiency in the electric motor drive [29].

2. Simulation Model

In order to evaluate this one-stage heat pump, a system model has been developed and programmed in the Engineering Equation Solver (EES) software [30]. The simulation model is based on steady-state part models for each component of the cycle, as described by Bertsch and Groll [14], [16].

2.1. Basic assumptions

The following assumptions were made:

- Pressure drops in refrigerant lines and heat exchangers are neglected ($p_1 = p_4 = p_6$ and $p_2 = p_3 = p_5$).
- Refrigerant leaving the condenser is saturated liquid ($x_3 = 0$). Subcooling is established in the SHX.
- Refrigerant leaving the evaporator is saturated vapor ($x_6 = 1$). Superheating in the SHX is 5°C.
- Expansion is adiabatic leading to an isenthalpic expansion process ($h_4 = h_5$).
- Water and brine mass flows are in counter flow to the refrigerant R134a.
- Brine is a 30 w% ethylene glycol-water mixture (fluid properties calculated by brineprop2 in EES)

2.2. Heat exchanger model

Overall NTU-effectiveness models [31] are used to model the heat exchange rates in the water-cooled condenser, brine-heated evaporator, and tube-in-tube suction line heat exchanger (SHX), which provides fast calculation and reasonably good results. Table 2 shows the equations used to determine the water and brine mass flow rates, the overall heat transfer coefficients (UA-values), the effectiveness, and the NTU-values of the heat exchangers. The equations for the evaporator and condenser are similar, for the SHX the ε-NTU relation for counter-flow conditions is applied. Energy balances on the components calculate the heat capacities.

Table 2. NTU-effectiveness calculations for the condenser, evaporator and SHX.

Condenser	Evaporator	SHX
$\dot{Q}_{cond} = \dot{m} \cdot (h_2 - h_3)$	$\dot{Q}_{evap} = \dot{m} \cdot (h_1 - h_4)$	$\dot{Q}_{SHX} = \dot{m} \cdot (h_5 - h_6) = \dot{m} \cdot (h_3 - h_1)$
$\varepsilon_{cond} = 1 - e^{-NTU_{cond}}$	$\varepsilon_{evap} = 1 - e^{-NTU_{evap}}$	$\varepsilon_{SHX} = \frac{1 - e^{-NTU_{SHX}(1-C_{SHX,r})}}{1 - C_{SHX,r}\, e^{-NTU_{SHX}(1-C_{SHX,r})}}$
$NTU_{cond} = UA_{cond} / (\dot{m}_{sink} \cdot c_{P,sink})$	$NTU_{evap} = UA_{evap} / (\dot{m}_{source} \cdot c_{P,source})$	$C_{SHX,r} = (\dot{m} \cdot c_{P,6}) / (\dot{m} \cdot c_{P,3}) < 1$

$$\dot{Q}_{cond} = \varepsilon_{cond} \cdot \dot{m}_{sink} \cdot c_{P,sink} \left(T_{cond} - T_{sink,in}\right) \qquad \dot{Q}_{evap} = \varepsilon_{evap} \cdot \dot{m}_{source} \cdot c_{P,source} \left(T_{source,in} - T_{evap}\right) \qquad NTU_{SHX} = UA_{SHX} / \left(\dot{m} \cdot c_{P,6}\right)$$

$$\dot{Q}_{cond} = \dot{m}_{sink} \cdot c_{P,sink} \cdot \left(T_{sink,out} - T_{sink,in}\right) \qquad \dot{Q}_{evap} = \dot{m}_{evap} \cdot c_{P,evap} \cdot \left(T_{evap,in} - T_{evap,out}\right) \qquad \dot{Q}_{SHX} = \varepsilon_{SHX} \cdot \dot{m} \cdot c_{P,6} \cdot \left(T_3 - T_6\right)$$

Figure 2 illustrates the selected temperature profiles at the design point conditions with the corresponding approach temperatures across the heat exchangers and the temperature differences between inlets and outlets. Table 3 summarizes the determined mass flow rates, heat transfer coefficients, effectiveness, NTU, and heat capacities at the design point. In the simulation, the UA-values and the flow rates were kept constant.

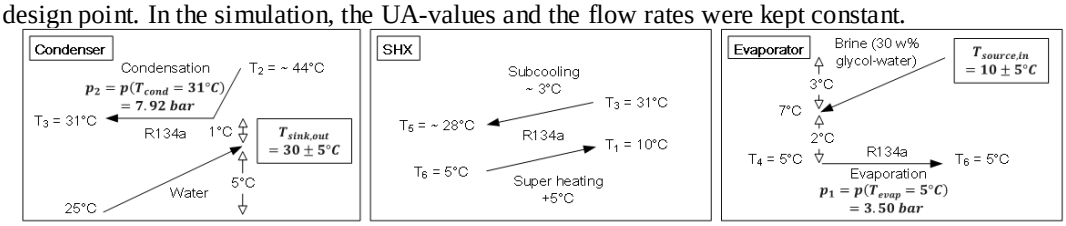

Fig. 2. Temperature profiles in the heat exchangers at the design point with approach temperatures and temperature differences.

Table 3. Mass flow rates, UA-values, effectiveness, NTU, and heat capacities at design point conditions.

Parameter	Parameter	Unit	Condenser	Evaporator	SHX
$\dot{m}$	water (brine) mass flow rates	kg/s	0.19	0.32	-
UA	heat transfer coefficient	kW/K	1.43	1.10	0.0045
ε	effectiveness	-	0.83	0.60	0.19
NTU	number of transfer units	-	1.79	0.92	0.23
$\dot{Q}$	heat capacity	kW	4.00	3.61	0.10

2.3. Compressor model

As the compressor characteristics depend on the inlet pressure, the inlet temperature, and the physical properties of the refrigerant, dimensional analysis is used to combine the involved fundamental parameters $(\dot{m}, \Pi, n, \eta)$ to non-dimensional numbers (M, Π, N, η) (Dixon and Hall [32]) (see Table 4).

Table 4. Non-dimensional numbers used to plot the compressor map.

Non-dimensional number	
Non-dimensional mass flow rate	$M = \dot{m}/\rho_1 a_1 D^2$
Non-dimensional rotational speed	$N = nD/a$
Pressure ratio	$\Pi = p_2/p_1$
Isentropic compressor efficiency	$\eta = (h_{2s} - h_1)/(h_2 - h_1)$

The compressor model used, is based on the predicted compressor map data of Javed et al. [22], [26]. Polynomial fit approximations derived from linear regression calculations are used to fit the compressor map data in the simulation model (see equations 1 and 2). Table 5 lists the corresponding coefficients $A_{0\ldots5}$ and $B_{0\ldots8}$. The R-squared values achieved are $R^2 > 99\%$.

$$\Pi = A_0 N + A_1 N^2 + A_2 MN + A_3 M^2 N + A_4 MN^2 + A_5 N^3 \quad (1)$$

$$\eta = B_0 + B_1 M + B_2 N + B_3 M^2 + B_4 N^2 + B_5 MN + B_6 M^2 N + B_7 MN^2 + B_8 N^3 \quad (2)$$

Table 5. Coefficients of the polynomial fits to map the pressure ratio and isentropic efficiency of the turbocompressor

Indices	0	1	2	3	4	5	6	7	8	R^2
A	9.71423	-27.4088	-13.2626	-1125.75	199.798	41.8093				0.99994
B	0.644742	-11.4222	1.85073	-852.193	-16.2465	239.349	1613.54	-406.352	23.8661	0.99635

3. Simulation Results

3.1. COP calculations

The performance of the heat pump is evaluated by calculating the heating coefficient of performance (COP)

$$COP = \dot{Q}_{cond} / W_{el} \tag{3}$$

whereas the electrical power consumed by the turbocompressor is

$$W_{el} = (h_2 - h_1) \tag{4}$$

The 2nd law efficiency is calculated by the ratio of the heating COP and the Carnot COP (theoretical max.):

$$\eta_{2nd} = COP / COP_{Carnot} \tag{5}$$

$$COP_{Carnot} = T_{sink,out} / \left(T_{sink,out} - T_{source,in}\right) \tag{6}$$

The graphs in Figure 3 show the influence of the different process parameters on the simulated heating COP and 2nd law efficiency. The COP increases with higher source temperature ($T_{source,in}$), lower sink temperature ($T_{sink,out}$) and lower heating capacity ($\dot{Q}_{cond}$). At the design point conditions (4.0 kW, B10°C/W30°C), a COP of 8.1 is reached with a 2nd law efficiency (η_{2nd}) of 53.4%. Within the studied operating conditions the 2nd law efficiency remains between 50% and 55%, which is high given the low temperature lift of the system (source to sink).

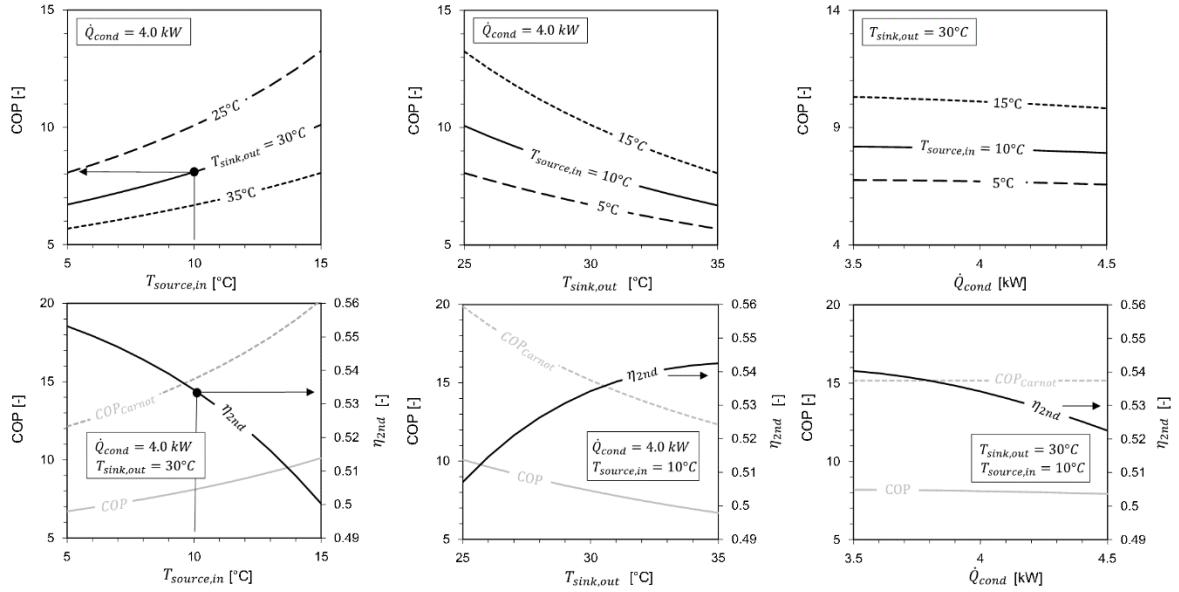

Fig. 3. Influence of the process parameters $T_{source,in}$, $T_{sink,out}$ and $\dot{Q}_{cond}$ on the heating COP and the 2nd law efficiency.

3.2. Heat pump operating range

Figure 4 illustrates the predicted and fitted compressor maps for the turbocompressor. The maximal achievable pressure ratio is about 3.5, which is limited by the maximal achievable rotational speed of 270 krpm (speed-line $N = 0.46$) and the small impeller size of 15.2 mm. As a reference, the black circle in the middle indicates the design point of the heat pump (HP), the rectangle the design point of the compressor. The grey dots reveal the area of isentropic efficiencies > 76%. In general, isentropic efficiencies of 72% to 77% are reached. The predicted surge and choke margins are also indicated.

The operating range of the cycle is evaluated by variation of each process parameter ($T_{source,in}$, $T_{sink,out}$, $\dot{Q}_{cond}$)

in its min/max limits (± variation range), while keeping the others constant. Table 5 shows the simulation results, including the design point conditions (HP). The operating points are plotted as black numbered dots (Figure 4, left). As can be seen, the operating points fit the map. The selected temperature levels of the evaporator and condenser define the required pressure ratio of the compressor. The highest temperature lift of 30°C (B5°C/W35°C, 4.5 kW, COP of 5.6) is illustrated by point ❹. A pressure ratio of about 3.2 is required. At 10°C ground heat, 4.0 kW of 30°C water is produced with a COP of 8.1 and 53.4% 2nd law efficiency (see HP design point).

Figure 4 (right) shows the results of the parametric study within the map. The arrows illustrate the results with increasing parameter value. The parameter variations move the operating point in the map towards the following main directions:

- $T_{source,in}$ $(5°C \rightarrow 15°C)$ to lower pressure ratio
- $T_{sink,out}$ $(25°C \rightarrow 35°C)$ to higher pressure ratio
- $\dot{Q}_{cond}$ $(3.5\ kW \rightarrow 4.5\ kW)$ to higher mass flow rates.

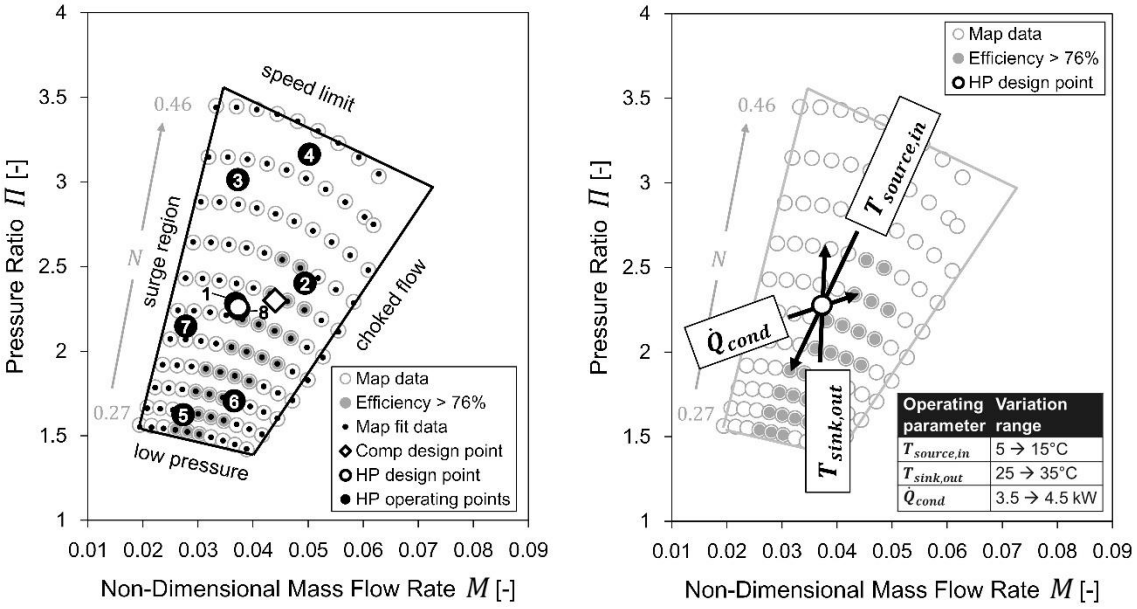

Fig. 4. Left: Predicted and fitted compressor map data with overlaid design and operating points according to Table 6. Right: Influence of the parametric variation study in the map (the arrows indicate increasing parameter value).

Table 5. Simulated operating points of the one-stage heat pump (numbers corresponds to the points in Figure 4, HP = design point).

no.	$T_{source.in}$ [°C]	$T_{sink.out}$ [°C]	$\dot{Q}_{cond}$ [kW]	COP [-]	η_{2nd} [%]	Π [-]	M [-]	$\dot{m}$ [g/s]	N [-]	n [rpm]	η [%]	$\dot{Q}_{evap}$ [kW]	W_{el} [kW]	T_{evap} [°C]	T_{cond} [°C]
❶	5	25	3.5	8.2	55.3	2.28	0.037	18.3	0.376	220877	75.7	3.17	0.42	0.6	25.9
❷	5	25	4.5	7.8	52.4	2.40	0.049	23.6	0.401	234844	76.2	4.03	0.58	-0.6	26.1
❸	5	35	3.5	5.7	55.4	3.01	0.037	18.5	0.436	257766	71.9	3.01	0.62	0.8	35.9
❹	5	35	4.5	5.6	54.7	3.16	0.050	24.1	0.455	267798	74.5	3.84	0.80	-0.3	36.1
❺	15	25	3.5	13.8	46.4	1.62	0.027	18.9	0.287	167048	76.2	3.30	0.25	10.4	25.9
❻	15	25	4.5	12.6	42.3	1.71	0.037	24.3	0.310	180118	76.5	4.21	0.36	9.2	26.1
❼	15	35	3.5	8.1	52.5	2.15	0.028	19.3	0.357	209156	72.5	3.16	0.43	10.6	35.9
❽	15	35	4.5	7.9	51.6	2.25	0.037	25.0	0.373	218121	76.0	4.04	0.57	9.4	36.1
HP	10	30	4	8.1	53.4	2.27	0.037	21.5	0.375	219643	75.9	3.61	0.49	5.0	31.0

4. Test set-up layout

Figure 5 presents the layout of the experimental test setup including the location of the measurement instrumentation. On the right, the 3D design is shown. The photo illustrates the design of the built impeller and gas bearings with herringbone grooves.

The water-cooled condenser and the brine-heated evaporator are plate-heat exchangers with a design capacity of 3.9 kW and 3.5 kW, respectively, considering high-efficiency heat transfer, compact and lightweight design. The SHX is a concentric tube-in-tube heat exchanger and enables superheating of the suction gas entering the compressor and subcooling the liquid leaving the condenser. At the outlet of the SHX the mass flow rate of the refrigerant is measured by a Coriolis flow meter. The filter drier traps particles and absorbs moisture from the line. The sight glass is used to check for sufficient refrigerant charge. The role of the SLA is to avoid small debris or liquid droplets from entering the compressor. This protection is especially important at startup and after changes in operating mode, especially during the first experiments. As an option, the SLA may be equipped with an electric heater to ensure complete liquid evaporation. The electronic expansion valve provides the pressure difference between the high and the low pressure and controls the superheat at the outlet of the SHX, i.e. at the inlet of the compressor. The discharge line has a check valve to prevent gas backflow to the compressor. Speed control of the turbocompressor modulates the mass flow rate and the achievable pressure ratio. The electrical power consumption of the motor is measured with a true RMS power meter. A water-glycol circuit provides the external cooling of the electric motor.

The bypass between the hot-gas and the suction line allows the compressor to start unloaded. The regulating bypass valve has a stepper motor to set the characteristic of the bypass. The solenoid valve is normally open and works as a safety measure to prevent surge when shutting-down the system. The regulating bypass valve is open during the starting period and is closed after the compressor is up to full speed. The gas bearing line uses high-pressure refrigerant, which is driven into the gas bearings and back to the suction line. The fine particulate filter in front of the gas bearing inlet protects the bearing section from small dusts that could block the grooves. A manual regulating valve is used to control the pressure at the bearing inlet to ensure the correct refrigerant flow.

The whole heat pump setup provides the necessary temperature and pressure sensors at the required states. The temperature inside the evaporator is controlled via the heat source. The discharge pressure and the mass flow are controlled by the rotational speed of the turbocompressor, the position of the bypass valve, and the heat sink conditions. A Pressostat (high/low pressure switch device) works as a safety measure in case of over- or under pressure. The data acquisition runs on National Instruments CompactRIO with modules for the different input and output signals in combination with LabVIEW software as user interface and for process monitoring. Closed heating and cooling loops for the evaporator and the condenser are installed in order to change the flow rates and inlet temperatures independently of each other. The suction piping is designed in vertical position providing an additional trap for liquid droplets by gravity. Flexible metal hoses are installed at the compressor in- and outlet to absorb potential vibration transmission along the pipes. The piping sizes were selected according to the fluid velocity recommendations described in ASHRAE [33] ensuring proper refrigerant flow without excessive pressure drop. No oil management is required, which results in slightly larger tubing to improve efficiency.

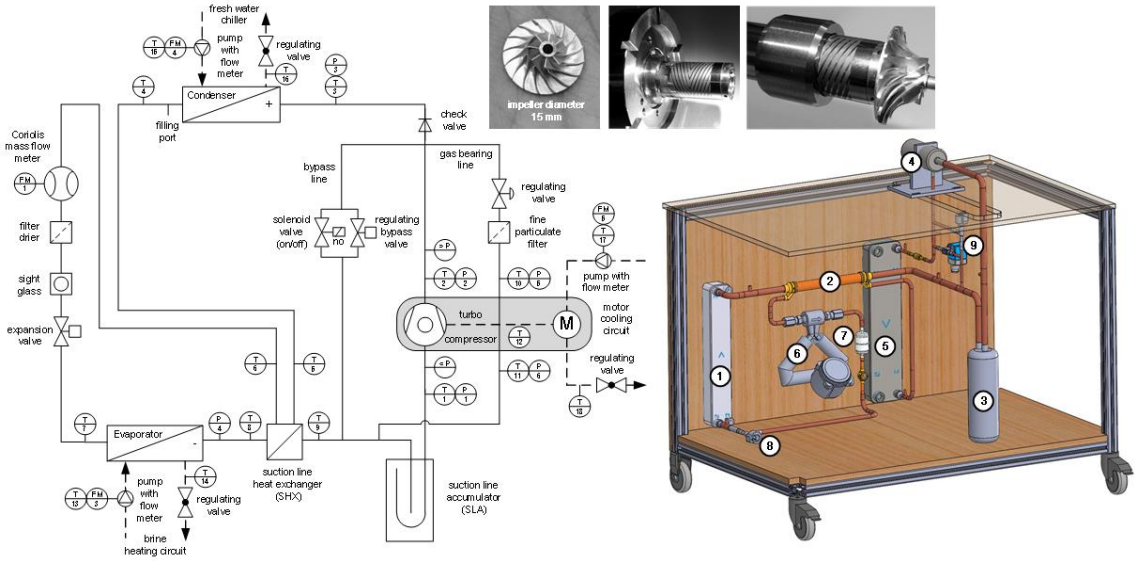

Fig. 5. Left: Test set-up of the one-stage heat pump with measurement instrumentation Right: 3D design of the test setup: (1) evaporator, (2) SHX, (3) SLA (separator), (4) turbo compressor, (5) condenser, (6) mass flow meter, (7) filter dryer and sight glass, (8) expansion valve, (9) bypass line (not shown: gas bearing line, cooling and heating circuits) Top: photos of the 15 mm impeller and gas bearings with herringbone grooves

5. Conclusions

A system model was developed and programmed in EES software in order to evaluate the performance of a one-stage heat pump cycle driven by a small-scale radial turbocompressor with 15.2 mm impeller diameter rotating on gas bearings optimized for R134a. The influence of the process parameters on the COP, the 2nd law efficiency and the operating conditions was studied. The simulation results reveal that the COP increases with higher source temperature, lower sink temperature and lower heating capacity. At the design point conditions (4.0 kW, B10°C/W30°C), a COP of 8.1 is reached with a 2nd law efficiency of 53.4%, which is high given the low temperature lift. The parameter study shows that the selected operating range of the heat pump fits the compressor map. As a continuation of this project an experimental testing prototype will be set up based on the developed simulation model and design layout.

First experimental measurement results are expected in the beginning of 2017. The system will serve as a proof of concept before stepping forward to a two-stage heat pump cycle with two separately driven turbocompressors reaching sink temperatures of 55 to 65°C [25]. The proposed two-stage system allows integration of a second heat source at intermediate temperature level, e.g. for solar heat or waste heat, providing significant COP improvements of 20% to 30% compared to a cycle without second heat source.

Acknowledgements

The authors thank the Swiss Competence Center for Energy Research on Efficiency of Industrial Processes (SCCER EIP) for their financial support.

Nomenclature

a	speed of sound	(m/s)	W	electrical compressor power	(kW)
c	heat capacity	(kJ/kg K)	x	refrigerant quality	(–)
COP	coefficient of performance	(–)	ε	effectiveness	(–)
D	tip diameter of the impeller	(m)	ρ	density at compressor inlet	(kg/m^3)
FM	flow meter		Π	pressure ratio	(–)
h	specific enthalpy	(kJ/kg)	η	isentropic efficiency	(–)
M	non-dimensional mass flow rate	(–)			

$\dot{m}$	mass flow rate	(kg/s)	**Subscripts**	
n	rotational speed	(rpm)	*cond*	condenser
NTU	number of transfer units	(–)	*el*	electrical
N	non-dimensional rotational speed	(–)	*evap*	evaporator
p	pressure	(kPa)	*in*	inlet
$\dot{Q}$	heat capacity	(kW)	*out*	outlet
SLA	suction line accumulator	(–)	*sink*	heat sink at the condenser
SHX	suction line heat exchanger	(–)	*source*	heat source at the evaporator
T	temperature	(°C)	*1 ... 6*	thermodynamic states
UA	UA-value	(kW/K)	*1 ... 9*	no. of operating points

References

[1] IEA, "Worldwide Trends in Energy Use and Efficiency." pp. 1–94, 2008.

[2] M. Eschmann, "Qualitätsüberwachung von Kleinwärmepumpen und statistische Auswertung 2015, Jahresbericht, Projektnummer: SI/401321-01." pp. 1–24, 2015.

[3] EHPA, "EHPA Testing Regulation: Testing of Water/Water and Brine/Water Heat Pumps based on EN 14511-1 to 14511-4 and EN 12102, Version 1.5, Release 01.09.2012." pp. 1–10, 2012.

[4] S. Renz, "Forschungsprogramm Wärmepumpen und Kältetechnik: Schwerpunkte 2013-16, in 19. Tagung des BFE-Forschungsprogramms 'Wärmepumpen und Kälte.'" pp. 9–21, 2013.

[5] M. Zehnder, "Efficient Air-Water Heat Pumps for High Temperature Lift Residential Heating, including oil migration aspects," Thèse N° 2998, EPFL, Switzerland, 2004.

[6] J. Schiffmann and D. Favrat, "High-Speed Low Power Radial Turbocompressor for Oil-Free Heat Pumps, Paper 1828," *Int. Compress. Eng. Conf.*, 2006.

[7] S. Hix, "Efficiency Comparison of Scroll vs . Reciprocating Technology in Different Climates, Bristol Compressors International, Inc., EWD001 EN X07401." pp. 1–3, 2016.

[8] C. Cuevas, J. Lebrun, V. Lemort, and E. Winandy, "Characterization of a scroll compressor under extended operating conditions," *Appl. Therm. Eng.*, vol. 30, no. 6–7, pp. 605–615, 2010.

[9] I. H. Bell, E. a. Groll, J. E. Braun, and W. T. Horton, "Experimental testing of an oil-flooded hermetic scroll compressor," *Int. J. Refrig.*, vol. 36, no. 7, pp. 1866–1873, 2013.

[10] Danfoss, "The Turbocor Family of Compressors Model TT300, Danfoss TURBOCOR," *Datasheet, www.turbocor.com, USA*, 2015.

[11] Friotherm AG, "Uniturbo 22 - Centrifugal Compressor for large scale refrigeration plants and heat pumps, Datasheet G001-05." pp. 1–2, 2005.

[12] J. Schiffmann and D. Favrat, "Design, experimental investigation and multi-objective optimization of a small-scale radial compressor for heat pump applications," *Energy*, vol. 35, no. 1, pp. 436–450, 2010.

[13] J. Schiffmann, "Small-Scale and Oil-Free Turbocompressor for Refrigeration Applications," *Int. Compress. Eng. Conf.*, vol. Paper 2354, 2014.

[14] S. S. Bertsch and E. A. Groll, "Air source heat pump for northern climates part I: simulation of different heat pump cycles, Paper 783," *Int. Refrig. Air Cond. Conf.*, pp. 1–9, 2006.

[15] C. Arpagaus, F. Bless, J. Schiffmann, and S. S. Bertsch, "Multi-temperature heat pumps: A literature review," *Int. J. Refrig.*, vol. 69, pp. 437–465, 2016.

[16] S. S. Bertsch and E. A. Groll, "Two-stage air-source heat pump for residential heating and cooling applications in northern U.S. climates," *Int. J. Refrig.*, vol. 31, no. 7, pp. 1282–1292, 2008.

[17] FISCHER Engineering Solutions AG, "Electric Micro-Turbo-Compressor EMTC-180k Ref, Datasheet." 2015.

[18] Celeroton AG, "Turbo Compressors with Gas Bearings, Brochure." pp. 1–7, 2016.

[19] J. Schiffmann, "Integrated Design and Multi-objective Optimization of a Single Stage Heat-Pump Turbocompressor," *J. Turbomach.*, vol. 137, no. 7, p. 071002, 2015.

[20] H. J. Van Gerner, G. Van Donk, A. Pauw, D. Krähenbühl, C. Zwyssig, and S. Lapensée, "A heat pump for space applications with a lightweight 200'000 rpm centrifugal three-stage compressor system," *ICR 2015, August 16-22, Yokohama, Japan*, p. ID: 12, pp. 1–8, 2015.

[21] I. Wyssen, L. Gasser, and B. Wellig, "Effiziente Niederhub-Wärmepumpen und -Klimakälteanlagen," in *19. Tagung des BFE-Forschungsprogramms "Wärmepumpen und Kälte,"* 2013, pp. 22–35.

[22] A. Javed, C. Arpagaus, S. Bertsch, and J. Schiffmann, "Small-scale turbocompressors for wide-range operation with large tip-clearances for a two-stage heat pump concept," *Int. J. Refrig.*, vol. 69, pp. 285–302, 2016.

[23] J. Schiffmann and D. Favrat, “Experimental investigation of a direct driven radial compressor for domestic heat pumps,” *Int. J. Refrig.*, vol. 32, no. 8, pp. 1918–1928, 2009.
[24] J. Carré, D. Favrat, and J. Schiffmann, “Experimental investigation of a two-stage oil-free domestic air/water heat pump prototype powered by an oil-free high-speed twin-stage radial compressor rotating on gas bearings, Paper 2219,” *16th Int. Refrig. Air Cond. Conf. Purdue, July 11-14*, pp. 1–10, 2016.
[25] C. Arpagaus, S. S. Bertsch, A. Javed, and J. Schiffmann, “Two-stage heat pump using oil-free turbocompressors – system design and simulation, Paper 2101,” *16th Int. Refrig. Air Cond. Conf. Purdue, July 11-14*, pp. 1–10, 2016.
[26] A. Javed, J. Schiffmann, C. Arpagaus, and S. Bertsch, “Design of oil-free turbocompressors for a two-stage industrial heat pump under variable operating conditions, Paper 1088,” *23rd Int. Compress. Eng. Conf. Purdue, July 11-14, 2016*, pp. 1–10, 2016.
[27] L. Gasser, B. Wellig, M. Bätschmann, and C. Meier, “Hocheffiziente Turbo-Wärmepumpe für Niederhub-Anwendungen,” in *18. Status-Seminar “Forschen für den Bau im Kontext von Energie und Umwelt,”* 2014, no. 4./5. September 2014, ETH Zürich, pp. 1–8.
[28] H. J. Van Gerner, G. Van Donk, A. Pauw, and J. Van Es, “A Heat Pump for Space Applications,” *45th Int. Conf. Environ. Syst.*, no. July, 12–16, Bellevue, Washington, pp. ICES–2015–35, pp. 1–13, 2015.
[29] J. Schiffmann, “Integrated Design, Optimization and Experimental Investigation of a Direct Driven Turbocompressor for Domestic Heat Pumps,” Thèse N° 4126, EPFL, Switzerland, 2008.
[30] S. A. Klein, “Engineering Equation Solver, Academic Professional V9.206, F-Chart Software.” 2012.
[31] S. A. Klein and G. Nellis, *Heat Transfer*. New York: Cambridge University Press, 2012.
[32] S. L. Dixon and C. A. Hall, *Fluid Mechanics and Thermodynamics of Turbomachinery, 7th edition*. Oxford, UK: Elsevier Inc., 2014.
[33] ASHRAE, “Chapter 1 - Halocarbon Refrigeration Systems,” in *Handbook - Refrigeration*, 2010.